A Hybrid FEM/MOM Technique for Electromagnetic Scattering and Radiation from Dielectric Objects with Attached Wires

Mohammad W. Ali, *Member, IEEE*, Todd H. Hubing, *Senior Member, IEEE*, and James L. Drewniak, *Member, IEEE*

***Abstract*— A hybrid formulation is presented, which combines the method of moments (MOM) with the edge-based vector finite element method (FEM) to solve electromagnetic radiation problems from structures consisting of an inhomogeneous dielectric body of arbitrary shape attached to one or more perfectly conducting bodies. While either method alone fails to model these structures efficiently, a combination of both finite element and moment methods provides an excellent way to solve these problems. The FEM is employed to handle the interior domain of inhomogeneous dielectric bodies and the method of moments is used to develop surface integrals that relate the field quantities on boundary surfaces with the equivalent surface currents. These integral equations are then coupled to the finite element equations through the continuity of the tangential magnetic fields across the hybrid boundaries.**

***Index Terms*— Electromagnetic modeling, electromagnetic interference, finite element method, method of moments.**

I. Introduction

NUMERICAL electromagnetic modeling (EM) has had a major impact on the way that high speed circuits and systems are designed. EM modeling codes are used to design everything from antennas to high-frequency circuits to components. There are a large number of computer programs available for analyzing various electromagnetic problems. These programs can be characterized by the technique they use to solve the complex equations associated with EM field analysis.

Surface integral techniques (e.g. the method of moments (MOM's) or the boundary element method) solve Maxwell's equations in their integral form. Surface integral techniques are very efficient at solving open radiation problems involving long thin wires and/or conducting surfaces. These techniques are often used to model resonant antennas or large resonant structures such as ships or aircraft. However, configurations with complex, arbitrary geometries (particularly those with inhomogeneous dielectrics) are not readily modeled using surface integral techniques.

Manuscript received September 16, 1996; revised July 9, 1997.

M. W. Ali is with the Carrier Systems Division, 3Com Corporation, Mount Prospect, IL 60056 USA.

T. H. Hubing and J. L. Drewniak are with the Department of Electrical Engineering, Electromagnetic Compatibility Laboratory, University of Missouri, Rolla, MO 65401 USA.

Publisher Item Identifier S 0018-9375(97)08421-4.

Numerical electromagnetic modeling techniques based on the solution of Maxwell's equations in their differential form are very good at modeling complex geometries with inhomogeneous dielectrics. Partial differential equation (PDE) techniques divide the region under analysis into elements or cells. Each cell can have it's own electromagnetic properties. The finite element method (FEM) and the finite difference time domain method are examples of PDE techniques.

The primary disadvantage associated with PDE techniques is their inability to efficiently model large unbounded radiating structures. The entire volume under analysis must be meshed and it is necessary to employ absorbing boundary elements at the outer surface of the meshed region in order to model unbounded geometries.

Since surface integral techniques excel at modeling the types of problems that PDE techniques do not model well and vice versa, several researchers have proposed combining a surface integral technique and a PDE technique in the same software [1]–[7]. These hybrid approaches take advantage of the strengths of each numerical technique in order to solve problems that neither technique alone could model efficiently.

This paper describes the development of a new hybrid numerical electromagnetic modeling technique. This work was motivated by the need to model electromagnetic interference (EMI) source configurations. EMI sources often contain regions that are highly complex and inhomogeneous [e.g. printed circuit boards (PCB's)] and regions with large conducting surfaces and/or wires (e.g. enclosures and cables). Since neither a surface integral technique nor a PDE technique alone can model this type of configuration effectively, a hybrid approach is required.

EMI source configurations usually involve a direct electrical connection between a highly inhomogeneous source region and a region with large conducting surfaces. Hybrid approaches previously described in the literature do not allow the continuity of current flow between the conducting surfaces and the inhomogeneous source region.

The approach described here combines a FEM with a moment method technique resulting in an algorithm that can use each technique to analyze the portions of the problem to which it is best suited. The new hybrid technique permits sources to be located anywhere within or outside of the finite-

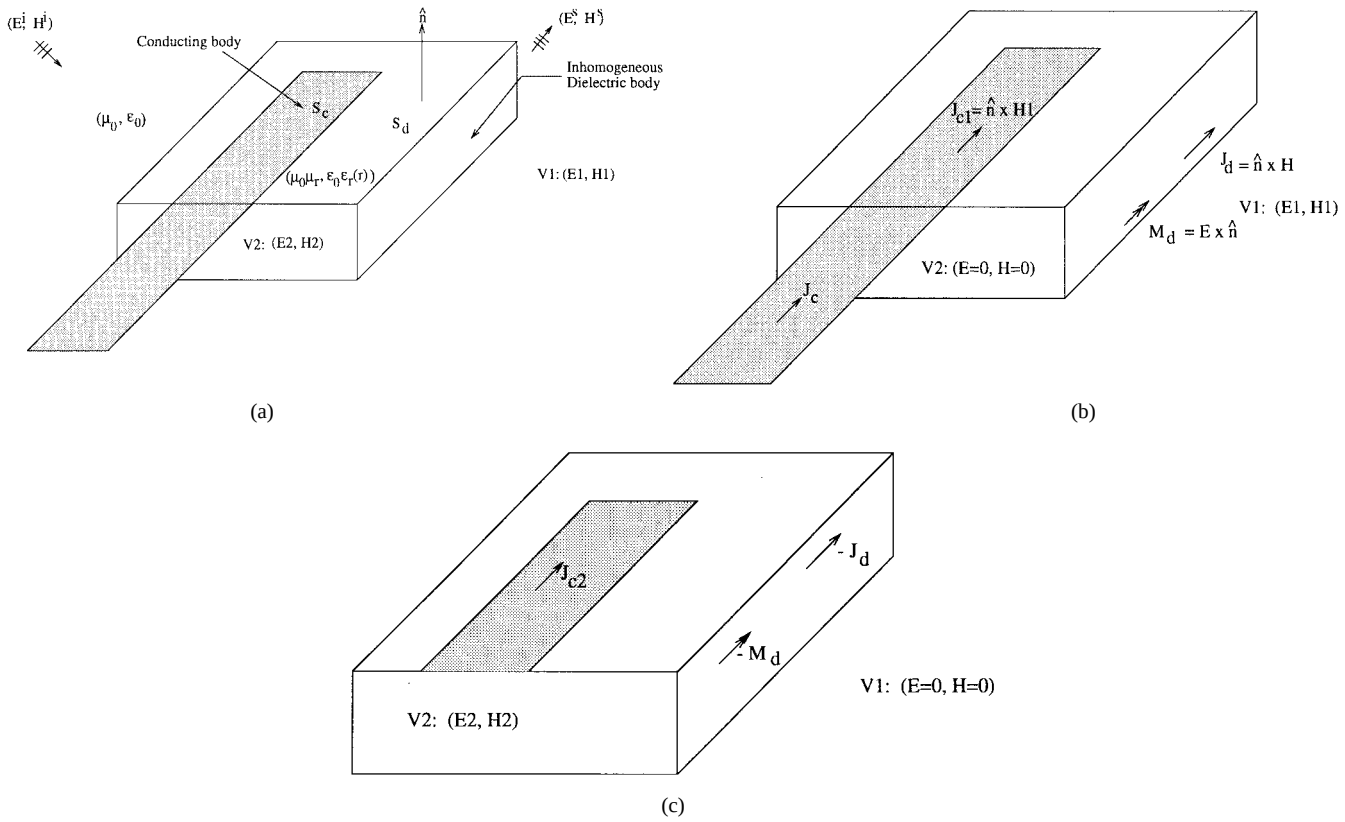

Fig. 1. Geometry of an inhomogeneous dielectric body attached to a conducting body: (a) the original problem, (b) its external equivalence, and (c) internal equivalence.

element region and it permits conducting surfaces to lie on or penetrate the boundary between the moment method and finite element regions.

For the finite element discretization, tetrahedral elements are chosen and an edge-based basis function is used. For the MOM surface integrals, the dielectric and/or conducting bodies are subdivided into triangular elements corresponding to the faces of the tetrahedrons. A triangular patch basis function developed by Rao *et al.* [11] is used to represent the equivalent currents at the boundaries. A unique feature of these basis functions is that they do not contain fictitious line or point electric charges that (especially at low frequencies) may be the dominant contributor to the electric field and may introduce serious errors. Also, the junction basis functions described in [21] are used to couple the dielectric bodies to the conducting wires.

This paper is organized as follows. Section II describes the theoretical formulation of the hybrid FEM-MOM approach. Section III explains how the FEM and MOM formulations are discretized and coupled. In Section IV, junction basis functions are added to the formulations allowing conductors to be modeled on the boundary between the FEM and MOM regions. Numerical results are presented in Section V. Section VI summarizes the primary results and conclusions that can be drawn from this work.

II. Formulation

In this section and the following three, we present the hybrid FEM-MOM formulation. Our goal is to develop the formulation for the structure shown in Fig. 1, where a conducting body touches the dielectric structure and extends beyond the dielectric-conductor interface. However, we first develop the formulation for the simpler structure, shown in Fig. 2, in order to more clearly demonstrate the application of the equivalence principles. The formulation for the structure in Fig. 1 is a slight modification of that for the structure in Fig. 2. This modification will be discussed in Section IV-A. Fig. 2 shows an inhomogeneous dielectric structure partially covered by a conducting body. The interior region of the dielectric structure is characterized by $[\mu_0\mu_r, \epsilon_0\epsilon_r(\boldsymbol{r})]$ and the exterior region by (μ_0, ϵ_0). μ_0 and ϵ_0 are the free space permeability and permittivity, respectively. The relative permeability is assumed to be constant in the dielectric structure. Since the dielectric region contains different materials, $\boldsymbol{r}$ is used to denote the spacial dependence. The structure can either be illuminated by an incident field $(\boldsymbol{E}^i, \boldsymbol{H}^i)$ or be excited by a source internal to the dielectric region. The formulation to be derived in the following subsections is generalized for both types of excitations. By introducing the equivalence principle, we separate the entire region V_0 $(= V_1 \cup V_2)$ into the two subregions shown in the lower portion of Fig. 2. The region external to the dielectric is denoted by V_1 and the region inside the dielectric is denoted by V_2. The regions are coupled through proper boundary conditions. For the interior region, the FEM is applied where the unknown boundary information is represented by equivalent electric currents $\boldsymbol{J}$ and the tangential electric field $\boldsymbol{E}$. For the exterior region, the method of moments is applied and a set of

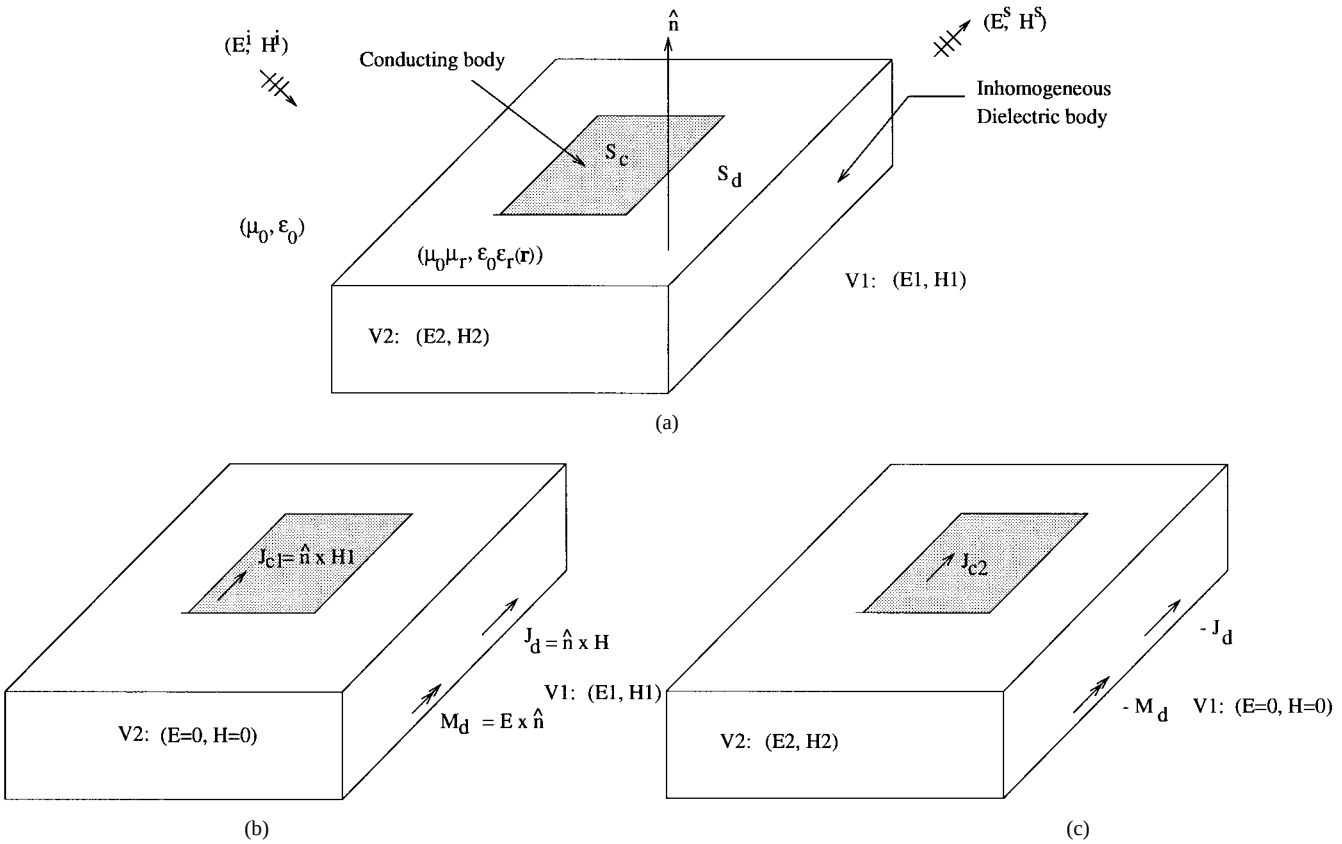

Fig. 2. Geometry of an inhomogeneous dielectric body partially covered by conductors: (a) the original problem, (b) its external equivalence, and (c) internal equivalence.

surface integral equations are developed for dielectric and conducting surfaces.

A. Finite Element Formulation

To derive the finite element formulation for the interior region V_2, we start with two basic Maxwell's equations that govern the time-harmonic EM fields in this region

$$\nabla \times \boldsymbol{E}(\boldsymbol{r}) = -\boldsymbol{M}^{\text{int}}(\boldsymbol{r}) - j\omega\mu_r\mu_0\boldsymbol{H}(\boldsymbol{r}) \tag{1}$$

$$\nabla \times \boldsymbol{H}(\boldsymbol{r}) = \boldsymbol{J}^{\text{int}}(\boldsymbol{r}) + j\omega\epsilon_r(\boldsymbol{r})\epsilon_0\boldsymbol{E}(\boldsymbol{r}) \tag{2}$$

where $\boldsymbol{J}^{\text{int}}$ and $\boldsymbol{M}^{\text{int}}$ are internal electric and magnetic sources respectively. From these equations, it is possible to eliminate one field variable and obtain a *curl curl* equation in terms of the other field variable

$$\nabla \times \left(\frac{1}{j\omega\mu_0\mu_r}\nabla \times \boldsymbol{E}(\boldsymbol{r})\right) + j\omega\epsilon_0\epsilon_r(\boldsymbol{r})\boldsymbol{E}(\boldsymbol{r}) = -\boldsymbol{J}^{\text{int}}(\boldsymbol{r}) - \frac{1}{j\omega\mu_0\mu_r}\nabla \times \boldsymbol{M}^{\text{int}}(\boldsymbol{r}) \tag{3}$$

$$\nabla \times \left(\frac{1}{j\omega\epsilon_r(\boldsymbol{r})\epsilon_0}\nabla \times \boldsymbol{H}(\boldsymbol{r})\right) + j\omega\mu_0\mu_r\boldsymbol{H}(\boldsymbol{r}) = -\boldsymbol{M}^{\text{int}}(\boldsymbol{r}) + \frac{1}{j\omega\epsilon_r(\boldsymbol{r})\epsilon_0}\nabla \times \boldsymbol{J}^{\text{int}}(\boldsymbol{r}). \tag{4}$$

Both (3) and (4) involve second derivatives. We can reduce them to single derivative expressions by constructing their weak forms. Multiplying (3) by a set of real *vector* weighting functions $\boldsymbol{w}(\boldsymbol{r})$, and integrating over the finite-element domain V_2, we obtain

$$\int_{V_2}\left[\nabla \times \left(\frac{1}{j\omega\mu_0\mu_r}\nabla \times \boldsymbol{E}(\boldsymbol{r})\right)\cdot\boldsymbol{w}(\boldsymbol{r}) + j\omega\epsilon_0\epsilon_r(\boldsymbol{r})\boldsymbol{E}(\boldsymbol{r})\cdot\boldsymbol{w}(\boldsymbol{r})\right]dV_2 = -\int_{\Omega}\left[\boldsymbol{J}^{\text{int}}(\boldsymbol{r})\cdot\boldsymbol{w}(\boldsymbol{r}) + \frac{1}{j\omega\mu_0\mu_r}\nabla \times \boldsymbol{M}^{\text{int}}(\boldsymbol{r})\cdot\boldsymbol{w}(\boldsymbol{r})\right]dV_2. \tag{5}$$

Using Stratton's first theorem

$$\int_V(\nabla \times \boldsymbol{a}\cdot\nabla \times \boldsymbol{b} - \boldsymbol{a}\cdot\nabla \times \nabla \times \boldsymbol{b})\,dV = \int_S[\boldsymbol{a}\times(\nabla \times \boldsymbol{b})]\cdot\hat{n}\,dS \tag{6}$$

and letting $\boldsymbol{a} = \boldsymbol{w}$, and $\nabla \times \boldsymbol{b} = (1/j\omega\mu_0\mu_r)\nabla \times \boldsymbol{E}$, yields a weak form [22] of (5)

$$\int_{V_2}\left(\frac{1}{j\omega\mu_o\mu_r}\nabla \times \boldsymbol{E}(\boldsymbol{r})\right)\cdot(\nabla \times \boldsymbol{w}(\boldsymbol{r})) + j\omega\epsilon_0\epsilon_r(\boldsymbol{r})\boldsymbol{E}(\boldsymbol{r})\cdot\boldsymbol{w}(\boldsymbol{r})\,dV_2 = \int_S(\hat{n}\times\boldsymbol{H}(\boldsymbol{r}))\cdot\boldsymbol{w}(\boldsymbol{r})\,dS - \int_{V_2}\left[\boldsymbol{J}^{\text{int}}(\boldsymbol{r}) + \frac{1}{j\omega\mu_0\mu_r}\nabla \times \boldsymbol{M}^{\text{int}}(\boldsymbol{r})\right]\cdot\boldsymbol{w}(\boldsymbol{r})\,dV_2. \tag{7}$$

This equation gives a relationship between the electric field inside the inhomogeneous medium and the tangential magnetic field at the boundaries.

B. Method of Moments Formulation

To derive the MOM formulation for our hybrid problem, we consider the external equivalence of Fig. 2. The total tangential components of electric field on surfaces S_d and S_c are obtained from the following surface $\boldsymbol{E}$ representation:

$$[E_d^1(J_d)+E_d^1(M_d)+E_d^1(J_{c1})+E_d^{\text{inc}}]_{\tan}=0 \tag{8}$$

$$[E_c^1(J_d)+E_c^1(M_d)+E_c^1(J_{c1})+E_c^{\text{inc}}]_{\tan}=0. \tag{9}$$

Since we use the electric field integral equation for our MOM formulation, the electric field $\boldsymbol{E}$ (after dropping the subscripts and superscripts representing the region) due to the electric current $\boldsymbol{J}$ and the magnetic current $\boldsymbol{M}$ is given by

$$\boldsymbol{E}(J,M)=-j\omega\boldsymbol{A}(\boldsymbol{r})-\nabla V(\boldsymbol{r})-\left(\frac{1}{\epsilon}\right)\nabla\times\boldsymbol{F}(\boldsymbol{r}) \tag{10}$$

where the vector potential functions $\boldsymbol{A}$ and $\boldsymbol{F}$ and the scalar potential function V are defined by

$$\boldsymbol{A}_d(\boldsymbol{r})=\mu_d\int_{S_d}\boldsymbol{J}_d(\boldsymbol{r}')G_0(\boldsymbol{r},\boldsymbol{r}')\,dS(\boldsymbol{r}') \tag{11}$$

$$V_d(\boldsymbol{r})=\frac{1}{\epsilon_d}\int_{S_d}\rho_d^e(\boldsymbol{r}')G_0(\boldsymbol{r},\boldsymbol{r}')\,dS(\boldsymbol{r}') \tag{12}$$

$$\boldsymbol{F}_d(\boldsymbol{r})=\epsilon_d\int_{S_d}\boldsymbol{M}_d(\boldsymbol{r}')G_0(\boldsymbol{r},\boldsymbol{r}')\,dS(\boldsymbol{r}') \tag{13}$$

for $\boldsymbol{r}'$ on S_d and

$$\boldsymbol{A}_c(\boldsymbol{r})=\mu_0\int_{S_c}\boldsymbol{J}_c(\boldsymbol{r}')G_0(\boldsymbol{r},\boldsymbol{r}')\,dS(\boldsymbol{r}') \tag{14}$$

$$V_c(\boldsymbol{r})=\frac{1}{\epsilon_0}\int_{S_c}\rho_c^e(\boldsymbol{r}')G_0(\boldsymbol{r},\boldsymbol{r}')\,dS(\boldsymbol{r}') \tag{15}$$

for $\boldsymbol{r}'$ on S_c. The vectors $\boldsymbol{r}$ and $\boldsymbol{r}'$ are the source and observation points, respectively, and

$$G_0(\boldsymbol{r},\boldsymbol{r}')=\frac{e^{-jk_0|\boldsymbol{r}-\boldsymbol{r}'|}}{4\pi|\boldsymbol{r}-\boldsymbol{r}'|} \tag{16}$$

is the free space Green's function.

The equivalent electric and magnetic currents on surfaces S_d and S_c are related to the total electric and magnetic fields on the surface

$$\boldsymbol{J}_d(\boldsymbol{r}')=\hat{n}\times\boldsymbol{H}(\boldsymbol{r}')|S_d \tag{17}$$

$$\boldsymbol{M}_d(\boldsymbol{r}')=\boldsymbol{E}(\boldsymbol{r}')\times\hat{n}|_{S_d} \tag{18}$$

$$\boldsymbol{J}_c(\boldsymbol{r}')=\hat{n}\times\boldsymbol{H}(\boldsymbol{r}')|_{S_c} \tag{19}$$

where $\hat{n}$ is an outward unit normal on surfaces shown in Fig. 2. The equivalent electric charges are related to the currents by the continuity relations

$$\rho_d^e(\boldsymbol{r}')=\frac{-1}{j\omega}\nabla_s'\cdot\boldsymbol{J}_d(\boldsymbol{r}'),\quad \rho_c^e(\boldsymbol{r}')=\frac{-1}{j\omega}\nabla_s'\cdot\boldsymbol{J}_c(\boldsymbol{r}').$$

Using (9)–(19) we obtain

$$\begin{aligned}\boldsymbol{E}_d^{\text{inc}}(\boldsymbol{r})=\int_{S_d}\{&[\hat{n}'\times\boldsymbol{E}(\boldsymbol{r}')]\times\nabla'G_0(\boldsymbol{r},\boldsymbol{r}')\\&+jk_0\eta_0(\hat{n}'\times\boldsymbol{H}(\boldsymbol{r}'))G_0(\boldsymbol{r},\boldsymbol{r}')\\&+\frac{j\eta_o}{k_0}\nabla'\cdot(\hat{n}'\times\boldsymbol{H}(\boldsymbol{r}'))\nabla G_0(\boldsymbol{r},\boldsymbol{r}')\}\,dS'\end{aligned} \tag{20}$$

$$\begin{aligned}\boldsymbol{E}_c^{\text{inc}}(\boldsymbol{r})=-\int_{S_c}\{&[\boldsymbol{E}(\boldsymbol{r}')\times\hat{n}']\times\nabla'G_0(\boldsymbol{r},\boldsymbol{r}')\\&+jk_0\eta_0(\hat{n}'\times\boldsymbol{H}(\boldsymbol{r}'))G_0(\boldsymbol{r},\boldsymbol{r}')\\&+\frac{j\eta_0}{k_0}\nabla'\cdot(\hat{n}'\times\boldsymbol{H}(\boldsymbol{r}'))\nabla G_0(\boldsymbol{r},\boldsymbol{r}')\}\,dS'.\end{aligned} \tag{21}$$

These equations provide a relationship between the unknown tangential magnetic field quantities $\hat{n}\times\boldsymbol{H}$ and the unknown electric field quantities $\boldsymbol{E}\times\hat{n}$ on the boundary surfaces S_d and S_c.

III. Discretization

In this section, the discretization of both the finite element weak form and the MOM surface integrals are described. Linear tetrahedral elements have been chosen to be the basic building blocks in the finite element discretization. Triangular surface patches have been used to discretize the MOM surfaces. Prior to discretization, it is necessary to select suitable basis functions to expand the unknown quantities in the formulation.

A. Choice of Basis Functions

To avoid the possible occurrence of nonphysical solutions, a class of tangentially continuous finite "edge" elements, and consistent boundary surface elements are used. There are a number of different edge elements reported in the literature. For the interior domain of volume V_2, we chose the vector basis functions to be those proposed in [16]. They are defined within a tetrahedron and are associated with the six edges of the tetrahedron. Assuming the four nodes of a tetrahedron are numbered in a manner consistent with the left-hand rule and the edges are numbered as shown in Table I and Fig. 3, then the vector basis function associated with the kth edge of that tetrahedron is defined as

$$\boldsymbol{w}_k(\boldsymbol{r})=\begin{cases}\boldsymbol{f}_k+\boldsymbol{g}_k\times\boldsymbol{r} & \boldsymbol{r}\text{ in the tetrahedron}\\ 0 & \text{otherwise}\end{cases} \tag{22}$$

with

$$\boldsymbol{f}_k=\frac{b_k}{6V_e}(\boldsymbol{r}_{(7-k)_1}\times\boldsymbol{r}_{(7-k)_2}) \tag{23}$$

$$\boldsymbol{g}_k=\frac{b_kb_{7-k}}{6V_e}\boldsymbol{e}_{7-k} \tag{24}$$

where $k=1,2,\cdots,6$, and

$V_e=$ volume of the tetrahedron

$\boldsymbol{e}_k=\dfrac{(\boldsymbol{r}_{(7-k)_2}-\boldsymbol{r}_{(7-k)_1})}{b_k}=$ unit vector of the kth edge

$b_k=|(\boldsymbol{r}_{(7-k)_2}-\boldsymbol{r}_{(7-k)_1})|=$ length of the kth edge

TABLE I
NODE AND EDGE NUMBERING SCHEME OF A TETRAHEDRON

Edge#	k1	k2
1	1	2
2	1	3
3	1	4
4	2	3
5	4	2
6	3	4

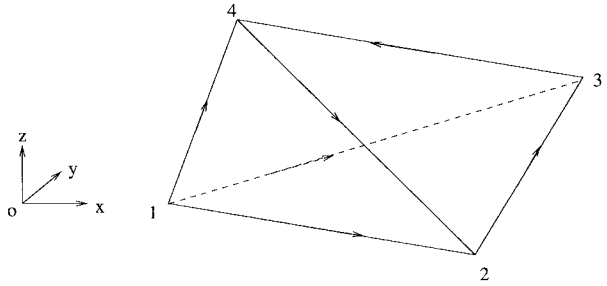

Fig. 3. Edge definition of a tetrahedron.

and $\boldsymbol{r}_{(7-k)_1}$ and $\boldsymbol{r}_{(7-k)_2}$ denote the location of the $(7-k)_1$ and $(7-k)_2$ nodes, respectively. A more detailed explanation of the basis function $\boldsymbol{w}_k$ can be found in [17].

Using these basis functions, the electric field $\boldsymbol{E}$ in the interior region can be expanded as

$$\boldsymbol{E}(\boldsymbol{r}) = \sum_{n=1}^{N_v} E_n \boldsymbol{w}_n(\boldsymbol{r}) \tag{25}$$

where $\{E_n, n = 1, 2, \cdots, N_v\}$ is a set of unknown complex scalars.

The expansion functions for the unknowns on the surface S_d and S_c are chosen to be those proposed in [11], which are given as

$$\boldsymbol{f}_n(\boldsymbol{r}) = \begin{cases} \dfrac{l_n}{2A_n^+}(\boldsymbol{r} - \boldsymbol{r}_n^+), & \boldsymbol{r} \text{ in } T_n^+ \\ \dfrac{l_n}{2A_n^-}(\boldsymbol{r}_n^- - \boldsymbol{r}), & \boldsymbol{r} \text{ in } T_n^- \\ 0, & \text{otherwise} \end{cases} \tag{26}$$

$$\nabla_S \cdot \boldsymbol{f}_n(\boldsymbol{r}) = \begin{cases} \dfrac{l_n}{A_n^+}, & \boldsymbol{r} \text{ in } T_n^+ \\ \dfrac{-l_n}{A_n^-}, & \boldsymbol{r} \text{ in } T_n^- \\ 0, & \text{otherwise} \end{cases} \tag{27}$$

where T_n^+ and T_n^- are two adjacent triangles with the nth edge common, l_n is the length of the nth common edge, $A_n^\pm$ is the area of the triangle $T_n^\pm$, and $\boldsymbol{r}^\pm$ are the position vectors of the node that are not related to the nth edge in triangle $T_n^\pm$. Fig. 4 shows the parameters associated with the basis function $\boldsymbol{f}_n$. The reader may refer to [11] and [18] for a detailed discussion on various properties of this basis function.

Using these basis functions, the unknown surface tangential field $\hat{n} \times \boldsymbol{H}$ can be expanded as

$$\hat{n} \times \boldsymbol{H}(\boldsymbol{r}) = \sum_{n=1}^{N_s} \mathcal{J}_n \boldsymbol{f}_n(\boldsymbol{r}). \tag{28}$$

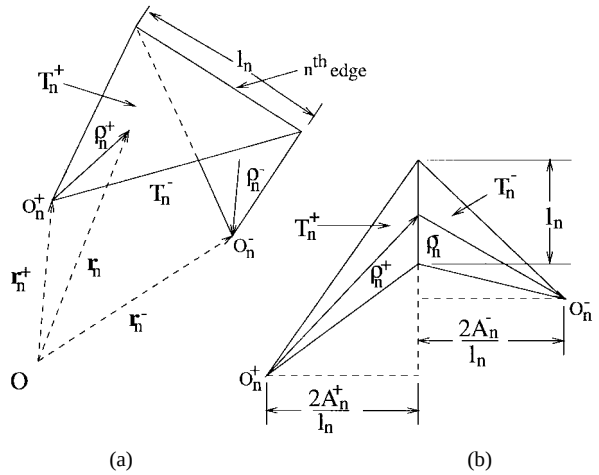

Fig. 4. (a) Coordinates of common edge associated with two triangles. (b) Geometry showing normal component of basis function at edge.

It can be shown that, on the boundary surface S, the basis functions $\boldsymbol{f}_n$ and $\boldsymbol{w}_n$ are related by

$$\boldsymbol{w}_n(\boldsymbol{r}) = \hat{n} \times \boldsymbol{f}_n(\boldsymbol{r})|_{\boldsymbol{r} \text{ on the surface } S}. \tag{29}$$

A description of this relationship can be found in [20, ch. 8].

B. Discretization of FEM Weak Form

To discretize the finite element interior region V_2, we divide the volume into several tetrahedral elements and use the volume basis function $\boldsymbol{w}(\boldsymbol{r})$ for expanding the state variable $\boldsymbol{E}$ in this region, and the surface basis function $\boldsymbol{f}(\boldsymbol{r})$ for expanding the intermediate quantity $\hat{n} \times \boldsymbol{H}$ on the boundary surface

$$\boldsymbol{E}(\boldsymbol{r}) = \sum_{n=1}^{N} E_n \boldsymbol{w}_n(\boldsymbol{r}) \tag{30}$$

$$\hat{n} \times \boldsymbol{H}(\boldsymbol{r}) = \sum_{n=1}^{N_d} J_n \boldsymbol{f}_n(\boldsymbol{r}). \tag{31}$$

If we use the Galerkin procedure for discretizing the weak form of the $\boldsymbol{E}$ formulation and assume the weighting functions to be the same as the expansion functions, then the discretized version of (7) becomes

$$[A]\{\mathcal{E}\} = [B]\{\mathcal{J}\} + \{\mathcal{G}^{\text{int}}\}. \tag{32}$$

The elements of $[A], [B]$, and $\{\mathcal{G}^{\text{int}}\}$ are

$$A_{mn} = \int_{V_2} \left[\frac{1}{j\omega\mu_0\mu_r} (\nabla \times \boldsymbol{w}_n(\boldsymbol{r})) \cdot (\nabla \times \boldsymbol{w}_m(\boldsymbol{r})) + j\omega\epsilon_0\epsilon_r \boldsymbol{w}_n(\boldsymbol{r}) \cdot \boldsymbol{w}_m(\boldsymbol{r}) \right] dV_2 \tag{33}$$

$$B_{mn} = \int_{S_d} \boldsymbol{f}_n(\boldsymbol{r}) \cdot \boldsymbol{w}_m(\boldsymbol{r})\, dS \tag{34}$$

$$\mathcal{G}_m^{\text{int}} = -\int_{V_2} \left[\boldsymbol{J}^{\text{int}} + \frac{1}{j\omega\mu_0\mu_r} \nabla \times \boldsymbol{M}^{\text{int}} \right] \cdot \boldsymbol{w}_m(\boldsymbol{r})\, dV_2 \tag{35}$$

where $[A]$ is a sparse, banded, and symmetric $N \times N$ matrix and $\{\mathcal{E}\}, \{\mathcal{G}^{\text{int}}\}$, and $\{\mathcal{J}\}$ are $N \times 1$ column vectors. Here, N is the total number of edges. The matrix $[B]$ is a sparse and

symmetric $N\times N$ matrix, where only the bottom-right $N_d\times N_d$ submatrix contains nonzero elements. N_d is the total number of edges on the dielectric boundary. The unknown electric field vector $\{\mathcal{E}\}$ consists of all field expansion coefficients with respect to the element edges interior to the finite element region.

C. Discretization of the MOM Surface Integrals

To discretize (20) and (21), we use (30) and (31) to expand the field quantities $\boldsymbol{E}(\boldsymbol{r})$ and $\hat{n}\times\boldsymbol{H}(\boldsymbol{r})$ respectively. Then testing these equations with the surface basis function $\boldsymbol{f}(\boldsymbol{r})$ and integrating over the boundary S gives

$$[C_{dd}]\{\mathcal{J}_d\}+[C_{dc}]\{\mathcal{J}_c\}=[D'_{dd}]\{\mathcal{E}_d\}-\mathcal{E}^i_d \tag{36}$$

$$[C_{cd}]\{\mathcal{J}_d\}+[C_{cc}]\{\mathcal{J}_c\}=[D'_{cd}]\{\mathcal{E}_d\}-\mathcal{E}^i_c. \tag{37}$$

The elements of the C and D matrices and the E vector are

$$c_{mn}-\left\langle\int_S\left[-jk_0\eta_0\boldsymbol{f}_n\boldsymbol{G}+\frac{j\eta_0}{k_0}\{\nabla'\cdot\boldsymbol{f}_n\}\nabla'\boldsymbol{G}\right]dS',\boldsymbol{f}_m\right\rangle \tag{38}$$

$$d'_{mn}=\left\langle\int_S[(\hat{n}'\times\boldsymbol{w}_n)\times\nabla'\boldsymbol{G}]\,dS',\boldsymbol{f}_m\right\rangle \tag{39}$$

$$e^i_m=\langle-\boldsymbol{E}^{\text{inc}},\boldsymbol{f}_m\rangle \tag{40}$$

where $C_{dd},C_{dc},C_{cd},C_{cc}$, and D'_{dd} are submatrices with dimensions $N_d\times N_d, N_d\times N_c, N_c\times N_d, N_c\times N_c, N_d\times N_d$, and $N_d\times N_c$, respectively. N_d and N_c are the total number of edges on S_d and S_c respectively.

Equation (39) involves a singularity when the source and observation points are located on the same surface patch. For such cases, we may evaluate the singularity contribution analytically [20, ch. 9], and doing this, (39) can be written as

$$\begin{aligned}d'_{mn}&=\tfrac{-1}{2}\int_S\boldsymbol{w}_m\cdot\boldsymbol{f}_m\,dS\\&\quad+\int_S\boldsymbol{f}_m\cdot\overline{\int_S}[(\hat{n}'\times\boldsymbol{w}_n)\times\nabla'\boldsymbol{G}]\,dS'\,dS\\&=\tfrac{1}{2}b_{mn}+d''_{mn}(\text{since }\langle\boldsymbol{w}_n,\boldsymbol{f}_m\rangle=-\langle\boldsymbol{f}_n,\boldsymbol{w}_m\rangle)\end{aligned} \tag{41}$$

where the bar across the integral indicates that the singular point has been removed. With the singularity removed, (36) and (37) become

$$\begin{aligned}&[C_{dd}]\{\mathcal{J}_d\}+[C_{dc}]\{\mathcal{J}_c\}\\&\quad=\tfrac{1}{2}[B_{dd}]\{\mathcal{E}_d\}+[D''_{dd}]\{\mathcal{E}_d\}-\mathcal{E}^i_d\end{aligned} \tag{42}$$

$$\begin{aligned}&[C_{cd}]\{\mathcal{J}_d\}+[C_{cc}]\{\mathcal{J}_c\}\\&\quad=\tfrac{1}{2}[B_{cd}]\{\mathcal{E}_d\}+[D''_{cd}]\{\mathcal{E}_d\}-\mathcal{E}^i_c\end{aligned} \tag{43}$$

which can be written more concisely as

$$[C_{dd}]\{\mathcal{J}_d\}+[C_{dc}]\{\mathcal{J}_c\}=[D_{dd}]\{\mathcal{E}_d\}-\mathcal{E}^i_d \tag{44}$$

$$[C_{cd}]\{\mathcal{J}_d\}+[C_{cc}]\{\mathcal{J}_c\}=[D_{cd}]\{\mathcal{E}_d\}-\mathcal{E}^i_c \tag{45}$$

where $D_{dd}=\frac{1}{2}B_{dd}+D''_{dd}$ and $D_{cd}=\frac{1}{2}B_{cd}+D''_{cd}$.

IV. Coupling

After partitioning the elements of matrices $[A]$ and $[B]$ in (7) for inner and boundary edges, and setting the tangential E field on the conducting walls to zero, we obtain the following form of the finite element equation

$$\begin{bmatrix}A_{ii}&A_{id}\\A_{di}&A_{dd}\end{bmatrix}\begin{Bmatrix}\mathcal{E}_i\\\mathcal{E}_d\end{Bmatrix}=\begin{bmatrix}0&0\\0&B_{dd}\end{bmatrix}\begin{Bmatrix}0\\\mathcal{J}_d\end{Bmatrix}+\begin{Bmatrix}0\\\mathcal{G}_i\end{Bmatrix} \tag{46}$$

where subscripts i and d refer to interior and boundary edges in the finite element volume V_2, respectively. Prior to coupling this equation with the MOM integrals, it is necessary to define the location of the source with respect to the volume V_2. The following two cases can be considered.

Case I) The source is outside of V_2: For this case, the last term in (46) is eliminated and the new equation becomes

$$\begin{bmatrix}A_{ii}&A_{id}\\A_{di}&A_{dd}\end{bmatrix}\begin{Bmatrix}\mathcal{E}_i\\\mathcal{E}_d\end{Bmatrix}=\begin{bmatrix}0&0\\0&B_{dd}\end{bmatrix}\begin{Bmatrix}0\\\mathcal{J}_d\end{Bmatrix}. \tag{47}$$

From (45), we obtain

$$\mathcal{J}_c=-C^{-1}_{cc}C_{cd}\mathcal{J}_d+C^{-1}_{cc}D_{cd}\mathcal{E}_d-C^{-1}_{cc}\mathcal{E}^i_c. \tag{48}$$

Substituting the value of $\mathcal{J}_c$ from (48) into (44) one obtains

$$\begin{aligned}&[C_{dd}-C_{dc}C^{-1}_{cc}C_{cd}]\mathcal{J}_d\\&\quad=[D_{dd}-C_{dc}C^{-1}_{cc}D_{cd}]\mathcal{E}_d+C_{dc}C^{-1}_{cc}\mathcal{E}^i_c-\mathcal{E}^i_d.\end{aligned} \tag{49}$$

Solving for $\mathcal{J}_d$ yields

$$\begin{aligned}\mathcal{J}_d&=[C_{dd}-C_{dc}C^{-1}_{cc}C_{cd}]^{-1}[D_{dd}-C_{dc}C^{-1}_{cc}D_{cd}]\mathcal{E}_d\\&\quad+[C_{dd}-C_{dc}C^{-1}_{cc}C_{cd}]^{-1}(C_{dc}C^{-1}_{cc}\mathcal{E}^i_c-\mathcal{E}^i_d)\\&=[C'_{dd}]^{-1}[D'_{dd}]\mathcal{E}_d+[C'_{dd}]^{-1}(C_{dc}C^{-1}_{cc}\mathcal{E}^i_c-\mathcal{E}^i_d)\end{aligned} \tag{50}$$

where $C'_{dd}=C_{dd}-C_{dc}C^{-1}_{cc}C_{cd}$ and $D'_{dd}=D_{dd}-C_{dc}C^{-1}_{cc}D_{cd}$. In matrix form

$$\begin{aligned}\begin{Bmatrix}0\\\mathcal{J}_d\end{Bmatrix}&=\begin{bmatrix}0&0\\0&[C'_{dd}]^{-1}[D'_{dd}]\end{bmatrix}\begin{Bmatrix}0\\\mathcal{E}_d\end{Bmatrix}\\&\quad+\begin{Bmatrix}0\\[C'_{dd}]^{-1}(C_{dc}C^{-1}_{cc}\mathcal{E}^i_c-\mathcal{E}^i_d)\end{Bmatrix}.\end{aligned} \tag{51}$$

This equation can easily be coupled to the finite element equation (47). The resulting hybrid matrix equation becomes

$$\begin{bmatrix}A_{ii}&A_{id}\\A_{di}&A'_{dd}\end{bmatrix}\begin{Bmatrix}\mathcal{E}_i\\\mathcal{E}_d\end{Bmatrix}=\begin{Bmatrix}0\\\mathcal{E}^{src}\end{Bmatrix} \tag{52}$$

where $A'_{dd}=A_{dd}-B_{dd}[C'_{dd}]^{-1}[D'_{dd}]$ and $\mathcal{E}^{src}=B_{dd}[C'_{dd}]^{-1}(C_{dc}C^{-1}_{cc}\mathcal{E}^i_c-\mathcal{E}^i_d)$. Once the solution of (52) is available, one can easily obtain J_d and J_c from (50) and (48), respectively.

Case II) The source is inside V_2: In this case, (44) and (45) are simplified as

$$[C_{dd}]\{\mathcal{J}_d\}+[C_{dc}]\{\mathcal{J}_c\}=[D_{dd}\{\mathcal{E}_d\} \tag{53}$$

$$[C_{dd}]\{\mathcal{J}_d\}+[C_{cc}]\{\mathcal{J}_c\}=[D_{cd}]\{\mathcal{E}_d\}. \tag{54}$$

From (54)

$$\mathcal{J}_c=-C^{-1}_{cc}C_{cd}\mathcal{J}_d+C^{-1}_{cc}D_{cd}\mathcal{E}_d, \tag{55}$$

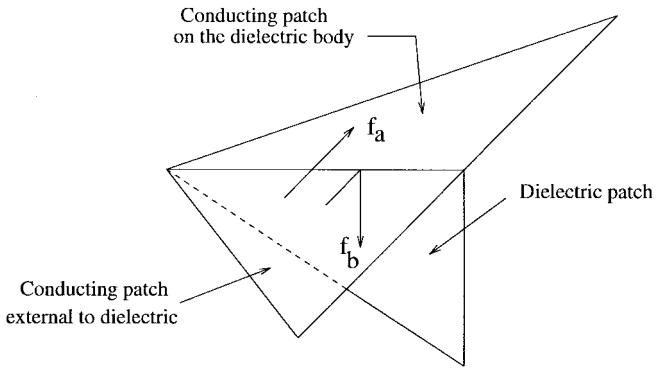

Fig. 5. Dielectric-conductor junction.

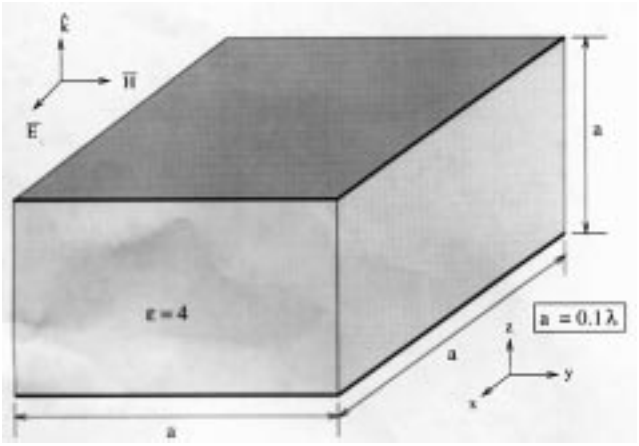

Fig. 6. Geometry of a dielectric box covered by two conducting plates placed on the top and bottom surfaces.

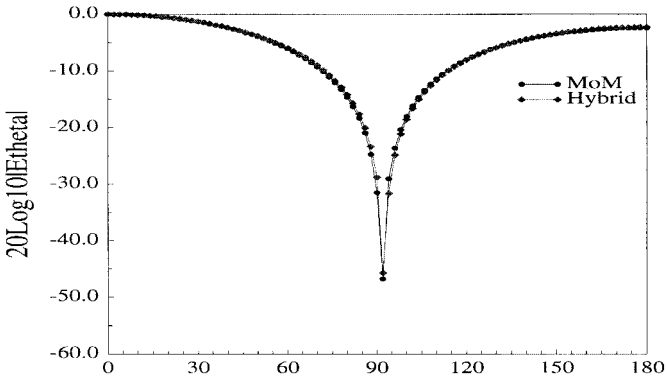

(a)

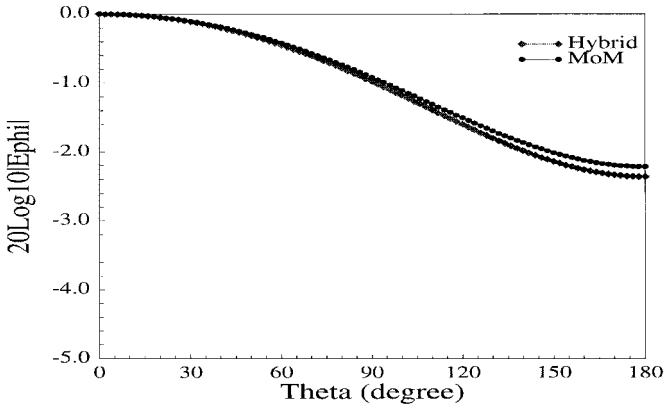

(b)

Fig. 7. Comparison for far fields: (a) 20 $\log_{10}|E_\theta|$ versus θ at $\phi = 0°$. (b) 20 $\log_{10}|E_\phi|$ versus θ at $\phi = 90°$.

Substituting the value of $\mathcal{J}_c$ from (55) into (53) one obtains

$$[C_{dd} - C_{dc}C_{cc}^{-1}C_{cd}]\mathcal{J}_d = [D_{dd} - C_{dc}C_{cc}^{-1}D_{cd}]\mathcal{E}_d. \quad (56)$$

Solving for $\mathcal{J}_d$ yields

$$\begin{aligned}\mathcal{J}_d &= [C_{dd} - C_{dc}C_{cc}^{-1}C_{cd}]^{-1}[D_{dd} - C_{dc}C_{cc}^{-1}D_{cd}]\mathcal{E}_d \\ &= [C'_{dd}]^{-1}[D'_{dd}]\mathcal{E}_d \end{aligned} \quad (57)$$

where $C'_{dd} = C_{dd} - C_{dc}C_{cc}^{-1}C_{cd}$ and $D'_{dd} = D_{dd} - C_{dc}C_{cc}^{-1}D_{cd}$. In matrix form

$$\begin{Bmatrix} 0 \\ \mathcal{J}_d \end{Bmatrix} = \begin{bmatrix} 0 & 0 \\ 0 & [C'_{dd}]^{-1}[D'_{dd}] \end{bmatrix} \begin{Bmatrix} 0 \\ \mathcal{E}_d \end{Bmatrix}. \quad (58)$$

This equation can easily be coupled to the finite element equation (46). The resulting hybrid matrix equation becomes

$$\begin{bmatrix} A_{ii} & A_{id} \\ A_{di} & A'_{dd} \end{bmatrix} \begin{Bmatrix} \mathcal{E}_i \\ \mathcal{E}_d \end{Bmatrix} = \begin{Bmatrix} 0 \\ \mathcal{G}^i \end{Bmatrix} \quad (59)$$

where $A'_{dd} = A_{dd} - B_{dd}[C'_{dd}]^{-1}[D'_{dd}]$. Once the solution of (59) is available, one can easily obtain J_d and J_c from (55) and (57), respectively.

A. Extended Hybrid Method

Now we extend the method developed in the previous sections to allow the conducting body to extend beyond the dielectric surface, as shown in Fig. 1. Using the equivalence principles, we obtain the interior and exterior equivalence shown in Fig. 1(b) and (c). The method of handling the interior region V_2 is identical to that described in the previous sections. However, the exterior equivalence is handled in a slightly different fashion. In this case, a "2-way" junction basis function [21] is used to represent the equivalent surface currents at dielectric-conductor junctions. For the type of junction shown in Fig. 1, two basis functions represent two types of current flowing across each junction edge. This is shown in Fig. 5. The basis function f_a represents the component of current that flows from the external conductor surface to the exterior surface of the dielectric-conductor interface. The basis function f_b represents the current component that flows into the dielectric body from the external conductor surface. These two currents are related in such a way that they obey Kirchhoff's current law and maintain current continuity at the junction. Since the current J_b represents the dielectric equivalent current at the junction, this current is set equal to the interior equivalent current corresponding to that edge.

V. Results

In this section, we present some numerical results obtained using the hybrid FEM-MOM technique described in the previous sections.

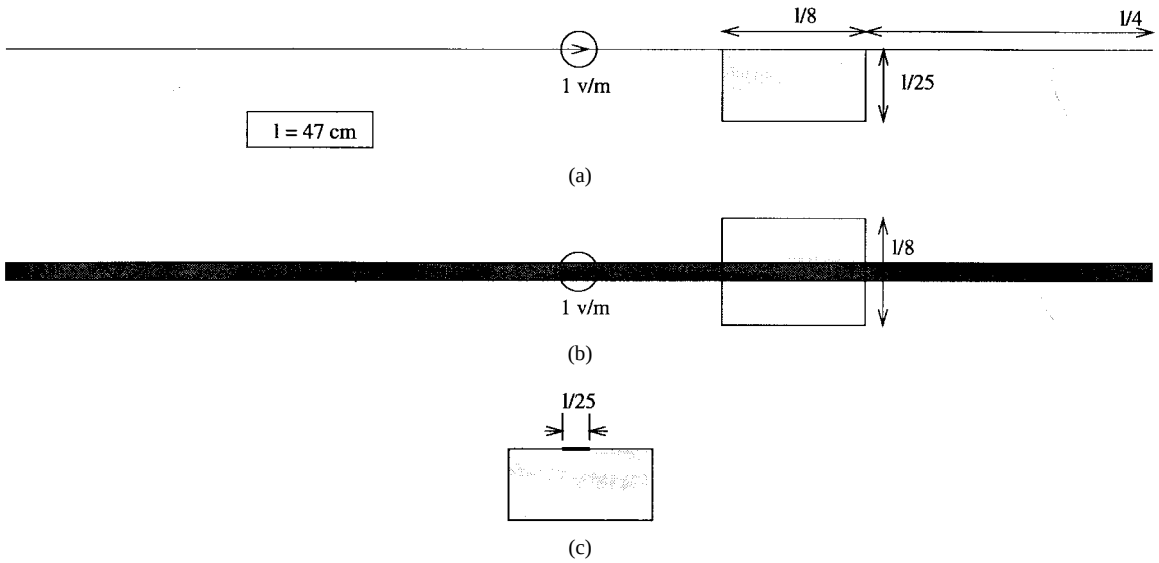

Fig. 8. Geometry of a center-fed dipole antenna placed on a dielectric box: (a) side view, (b) top view, and (c) front view.

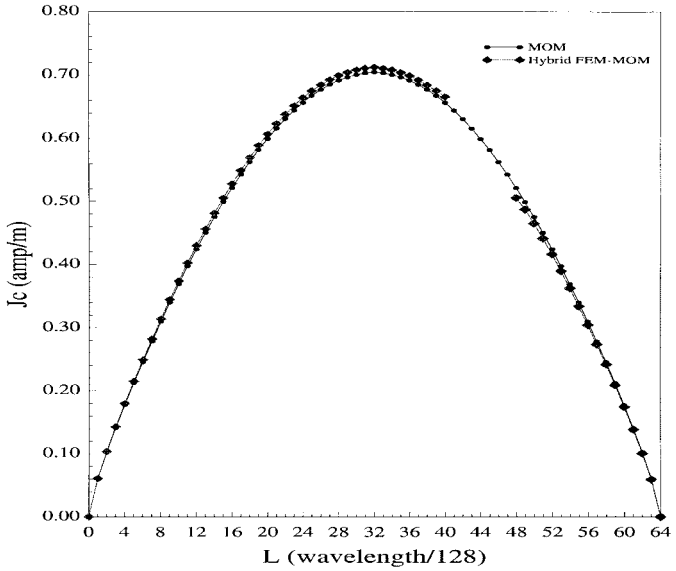

Fig. 9. Dipole current distribution at frequency 300 MHz.

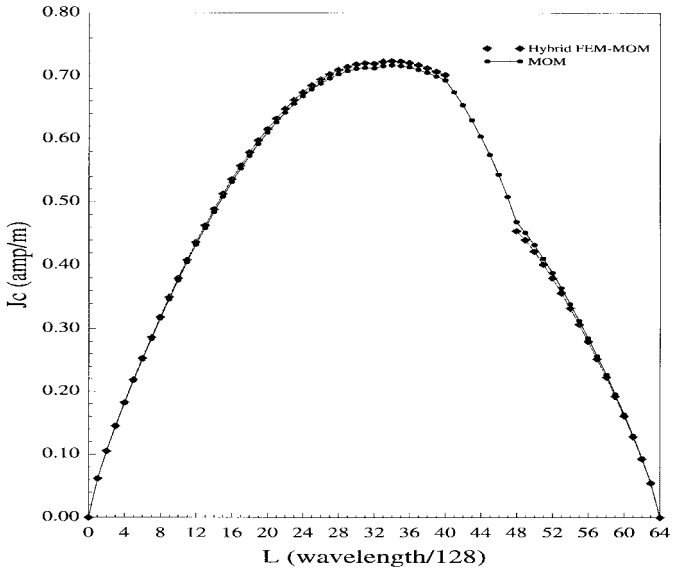

Fig. 10. Dipole current distribution in the presence of a dielectric box. Frequency $f = 300$ MHz.

A. Scattering by a Dielectric Body Partially Covered by a Conductor

As a first example, we consider the electromagnetic scattering from a 0.1 $\lambda\times$ 0.1 $\lambda\times$ 0.1 λ dielectric box ($\epsilon_r = 4.0$) covered by two conducting plates of dimension 0.1 $\lambda\times$ 0.1 λ. The conducting plates are placed on the top and bottom surfaces of the dielectric cube. The volume of the structure is discretized into 1280 tetrahedrons and the number of unknowns in the final hybrid matrix is 1684. The structure is illuminated by a normally incident plane wave as shown in Fig. 6. The scattered fields are plotted in Fig. 7 and compared with the results available in [24]. As is evident from the figures, the two solutions compare reasonably well.

B. Center-Fed Dipole Antenna Placed on an Air Dielectric Box

In this example, a center-fed dipole is placed on an air dielectric box with $\epsilon_r = 1.0$. This example demonstrates the ability of the proposed hybrid method to analyze the current behavior near the dielectric-conductor junctions. The configuration is shown in Fig. 8. Two cases are considered for this demonstration. In the first case, a center-fed dipole is placed on an air dielectric box with $\epsilon_r = 1.0$. The dipole is excited by a voltage source with magnitude 1 volt/meter. The length of the dipole is $\ell = 47$ cm and the width of the dipole is $\ell/25$. The dimensions of the dielectric box are $\ell/8 \times \ell/8 \times \ell/25$ and it is placed $\ell/8$ cm away from the center of the dipole. To discretize the model, the volume of the dielectric is divided into 480 tetrahedrons and the dipole is divided into 128 triangular patches. Theoretically, this box will have no effect on the current distribution along the dipole. Fig. 9 shows hybrid results for the current distribution at 300 MHz. For comparison, the current distribution at the same frequency obtained with a MOM formulation (no dielectric) is also provided. Very good agreement is obtained between

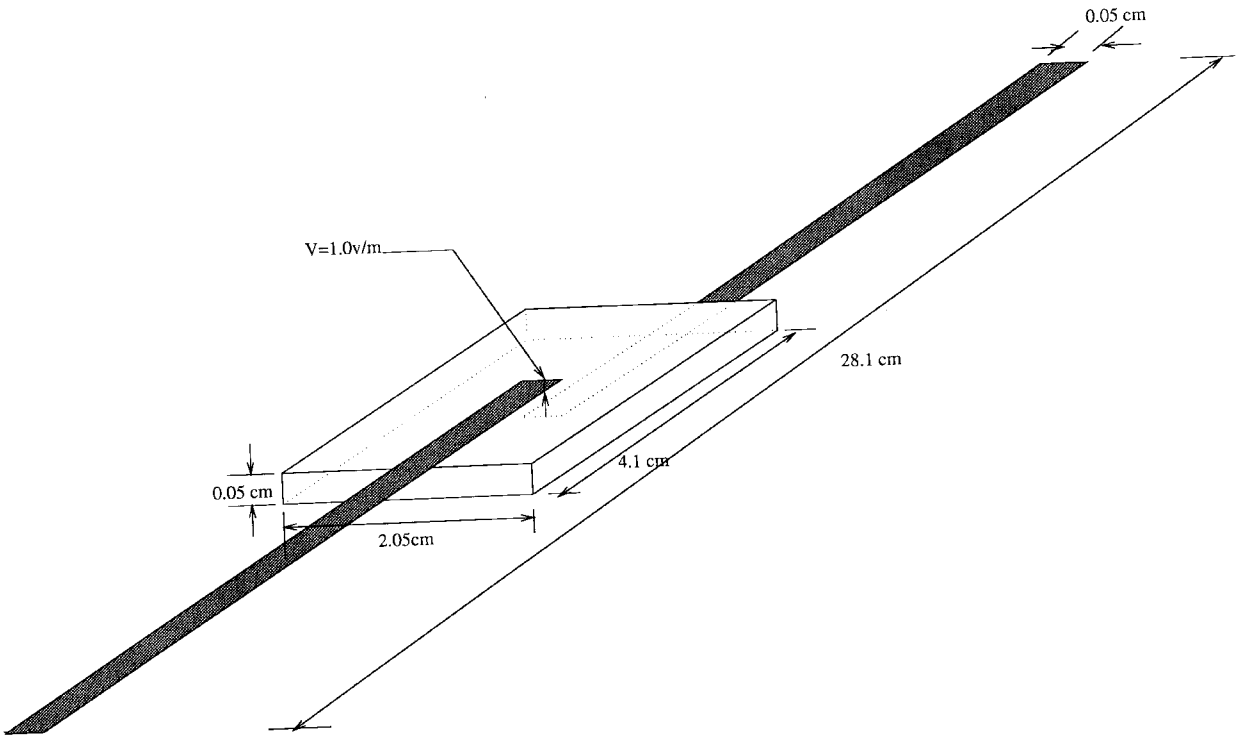

Fig. 11. Geometry of a simple PCB model.

the two results. Note that the hybrid method determines the equivalent currents exterior to and on the boundary of the finite element region. In the region where the dielectric box contacts the conductor surface, the hybrid method solves for the current on the topside of the conductor only. Currents on the underside of the conductor are part of the interior problem. Fig. 9 shows only the equivalent current values that correspond to actual currents. The hybrid approach could be used to find the actual currents on the conductor in the region where it contacts the dielectric surface by meshing the conductor-dielectric interface and solving for these values explicitly. This additional complexity is unnecessary however, since all of the interior and exterior field quantities can be determined from the equivalent currents on the boundary surfaces.

C. Center-Fed Dipole Antenna Placed on a Lossless Dielectric Box

In this example, the dielectric box used in the previous example is filled with a lossless dielectric material ($\epsilon_r = 4.0$). All other specifications are kept unchanged. This example illustrates the current behavior near the dielectric-conductor junction. The current distribution on the dipole is plotted in Fig. 10. For comparison, results from the MOM surface formulation [12] are also presented. The agreement between the two results is good.

D. PCB Dipole

The last example is the dipole antenna structure shown in Fig. 11. The model consists of a small printed circuit board (PCB) source that drives two quarter-wavelength traces. The primary difference between this configuration and those in the previous examples is that the source is located in the finite element region. When the relative permittivity of the dielectric in the finite element region is set to 1.0, the configuration is a half-wave dipole. The current distribution calculated using the hybrid code is shown in Fig. 12. For this calculation, the volume of the dielectric slab was divided into 1440 tetrahedrons and each off-board trace was divided into 48 triangular patches. The driving frequency was 533 MHz. Also plotted in Fig. 12, is the current distribution on a cylindrical dipole antenna with an equivalent wire radius [page 338, [23]] calculated using the numerical electromagnetics code (NEC). Fig. 13 shows the current distribution when the permittivity of the dielectric was set to 10.0. The results are compared to the currents calculated for the same configuration using the IBM Electromagnetic Simulator [8]. There are small differences in the peak current amplitude due to differences in the way that the voltage sources are implemented in the two models. In the hybrid model, voltage sources in the finite element region are implemented by forcing the electric field at one edge of an element. Voltage sources in the moment method region (and the voltages sources impressed by the IBM EM simulator) are applied to the face of an element. Field distributions in the vicinity of the source can affect the input impedance of the radiating structure.

VI. Conclusion

In this paper, a FEM-MOM hybrid method is presented and has been applied to the analysis of dielectric structures attached to conducting bodies. The hybrid method is capable of modeling structures with complex conductor-dielectric regions that would be difficult or impossible to model with a

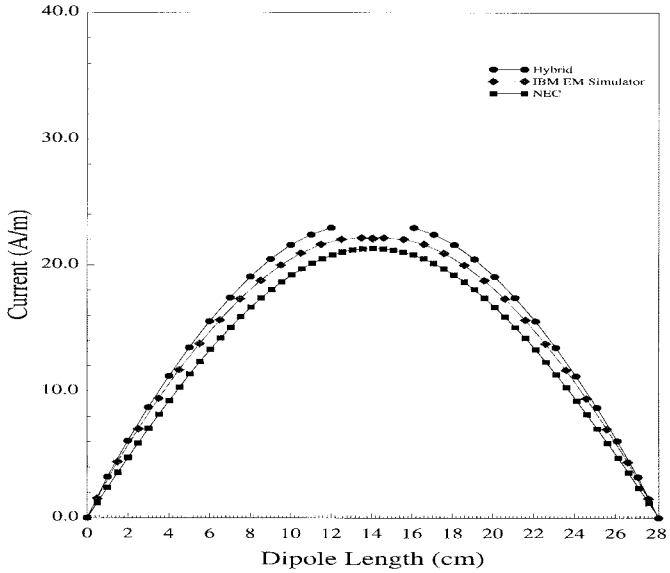

Fig. 12. Current distribution along the dipole length. $\epsilon_r = 1.0$. Frequency = 533 MHz.

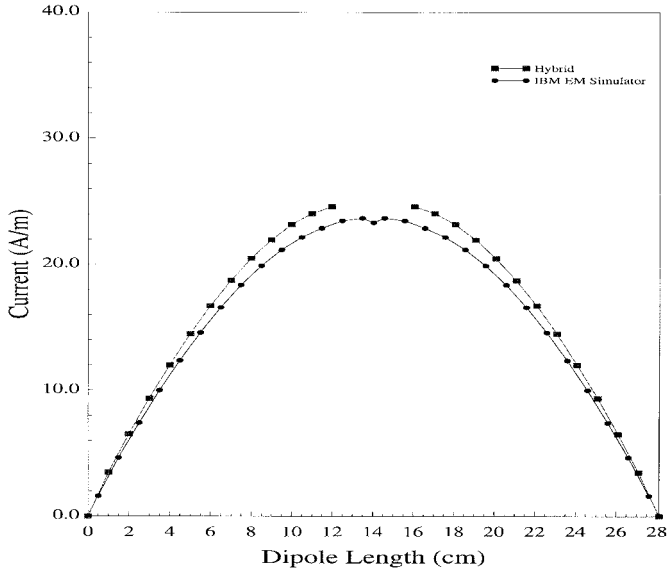

Fig. 13. Current distribution along the dipole length. $\epsilon_r = 10.0$. Frequency = 533 MHz.

moment method approach. The method also has advantages over FEM's employing absorbing boundary conditions. The fictitious boundaries, where the FEM interior regions couple to the MOM exterior regions, can be placed very near or directly on the surface of the radiating structures. The finite element analysis may be applied to highly inhomogeneous or complex regions of the problem while modeling long wires or large metal surfaces using the method of moments. Also, the incorporation of the junction basis functions to couple dielectric bodies to external wires and surfaces makes it possible to analyze structures where the wires or surfaces contact or penetrate the boundary between the two regions.

The technique described in this paper has been implemented and validated by modeling a number of simple structures and comparing the results obtained to theory and to results obtained using other numerical approaches.

ACKNOWLEDGMENT

The authors would like to thank S. Ji, University of Missouri, Rolla, for checking the equations in this manuscript and verifying the computation results, and the reviewers for their comments and helpful suggestions.

REFERENCES

[1] A. Taflove and K. Umashankar, "A hybrid moment method/finite-difference time-domain approach to electromagnetic coupling and aperture penetration into complex geometries," *IEEE Trans. Antennas Propagat.*, vol. AP-30, pp. 617–627, July 1982.

[2] J. Sroka, H. Baggenstos, and R. Ballisti, "On the coupling of the generalized multipole technique with the finite element method,," *IEEE Trans. Magn.*, vol. 26, pp. 658–661, Mar. 1990.

[3] J. M. Jin and J. L. Volakis, "A finite element-boundary integral formulation for scattering by three-dimensional cavity-backed apertures," *IEEE Trans. Antennas Propagat.*, vol. 39, pp. 97–104, Jan. 1991.

[4] W. E. Boyse and A. A. Seidl, "A hybrid finite element and moment method for electromagnetic scattering from inhomogeneous objects," in *Proc. 7th Ann. Rev. Progress Appl. Computat. Electromag.*, Mar. 1991, pp. 160–169.

[5] M. A. Morgan, C. H. Chen, S. C. Hill, and P. W. Barber, "Finite element-boundary integral formulation for electromagnetic scattering," *Wave Motion*, vol. 6, pp. 91–103, 1984.

[6] X. C. Yuan, D. R. Lynch, and J. W. Strohbehn, "Coupling of finite element and moment methods for electromagnetic scattering from inhomogeneous objects," *IEEE Trans. Antennas Propagat.*, vol. 38, pp. 386–393, Mar. 1990.

[7] X. C. Yuan, "Three-dimensional electromagnetic scattering from inhomogeneous objects by the hybrid moment and finite element method," *IEEE Trans. Microwave Theory Tech.*, vol. 38, pp. 1053–1058, Aug. 1990.

[8] S. Daijavad and B. J. Rubin, "Detailed analysis of a canonical structure in electromagnetic radiation problems," *IEEE Trans. Electromag. Compat.*, vol. 35, pp. 231–234, May 1993.

[9] ——, "Modeling common-mode radiation of 3D structures," *IEEE Trans. Electromag. Compat.*, vol. 34, pp. 57–61, Feb. 1992.

[10] B. J. Rubin and S. Daijavad, "Radiation and scattering from structures involving finite-sized dielectric regions," *IEEE Trans. Antennas Propagat.*, vol. 34, pp. 585–600, 1990.

[11] S. M. Rao, D. R. Wilton, and A. W. Glisson, "Electromagnetic scattering by surfaces of arbitrary shape," *IEEE Trans. Antennas Propagat.*, vol. AP-30, pp. 409–418, 1982.

[12] S. Ponnapalli, P. Midya, and H. Heeb, "Analysis of arbitrarily shaped three dimensional composite radiating structures using a method of moments surface formulation," to be published.

[13] D. Hockanson, J. L. Drewniak, T. H. Hubing, and T. P. Vandoren, "FDTD modeling of thin wire structures for simulating common-mode radiation from structures with attached cables," in *Proc. IEEE Electromag. Compat. Symp.*, Atlanta, GA, 1995, pp. 168–173.

[14] ——, "FDTD modeling of common-mode radiation from cables," in *IEEE Trans. Electromag. Compat.*, June 1995.

[15] A. Chattarjee, J. M. Jin, and J. L. Volakis, "Edge-based finite elements and vector ABC's applied to 3-D scattering," *IEEE Trans. Antennas Propagat.*, vol. 41, pp. 221–226, 1993.

[16] M. L. Barton and Z. J. Cendes, "New vector finite elements for three-dimensional magnetic field computation," *J. Appl. Phys.*, vol. 61, pp. 3919–3921, Apr. 1982.

[17] M. W. Ali, "Development of a hybrid 3D numerical modeling technique for analyzing printed circuit models with attached wires," Ph.D. dissertation, Univ. Missouri, Rolla, 1996.

[18] K. Umashankar, A. Taflove, and S. M. Rao, "Electromagnetic scattering by arbitrary shaped three-dimensional homogeneous lossy dielectric objects," *IEEE Trans. Antennas Propagat.*, vol. AP-34, June 1986.

[19] D. R. Wilton, S. M. Rao, A. W. Glisson, D. H. Schaubert, O. M. Al-Bundak, and C. M. Butler, "Potential integrals for uniform and linear source distributions on polygonal and polyhedral domains," *IEEE Trans. Antennas Propagat.*, vol. AP-32, Mar. 1984.

[20] J. Jin, *The Finite Element Method in Electromagnetics*. New York: McGraw-Hill, 1995.

[21] *Patch code User's Manual*. Houston, TX: Univ. Houston Press.

[22] J.-S. Wang, "On edge based finite elements and method of moments solutions of electromagnetic scattering and coupling," Ph.D. dissertation, University of Akron, OH, 1992.
[23] C. A. Balanis, "Antenna theory," *Analysis and Design*. New York: Harper, 1982.
[24] T. K. Sarkar, S. M. Rao, and A. R. Djordjevic, "Electromagnetic scattering and radiation from finite microstrip structures," *IEEE Trans. Microwave Theory Tech.*, vol. 38, Nov, 1990.

Mohammad W. Ali (S'95–M'96) was born in Jamalpur, Bangladesh on February 1, 1962. He received the B.S.E.E. degree from the Bangladesh University of Engineering and Technology, Dhaka, in 1987 and the M.S. and Ph.D. degrees in electrical engineering from the University of Missouri, Rolla, in 1992 and 1996, respectively.

From 1992 to 1996, he worked as a Graduate Research Assistant in the Electromagnetic Compatibility Laboratory, University of Missouri, Rolla, where he performed research on numerical modeling and analysis of printed circuit components. His graduate research was sponsored by the Interconnect Development group, Intel Corporation, OR. During the summer of 1993 and 1994, he worked at Intel Corporation as a Summer Intern. From 1996 to 1997, he worked for Standard Microsystems Corporation, Hauppauge, NY, where he engaged in research and development activity on PC and Networking products. In 1997, he joined the Carrier Systems Division, 3Com Corporation, Mount Prospect, IL, as an R&D engineer, and currently he is working on Signal Integrity and EMC issues on various netserver cards. His primary interests include numerical modeling, signal integrity, and EMC/EMI analysis of printed circuit boards.

Todd H. Hubing (S'82–M'83–SM'93), for a photograph and biograpy, see p. 155 of the May 1997 issue of this TRANSACTIONS.

James L. Drewniak (S'85–M'90), for a photograph and biograpy, see p. 155 of the May 1997 issue of this TRANSACTIONS.